Importin-β targets HURP to kinetochore-fibers in coordination with Ran-GTP in human mitotic cells

Kenta Tsuchiya[1], Hisato Hayashi[1], Momoko Nishina[1], Masako Okumura[1], Masato T. Kanemaki[2,3], Gohta Goshima[1], Tomomi Kiyomitsu[1,2]*

[1] Division of Biological Science, Graduate School of Science, Nagoya University, Chikusa-ku, Nagoya 464-8602, Japan.

[2] Precursory Research for Embryonic Science and Technology (PRESTO) Program, Japan Science and Technology Agency, 4-1-8 Honcho Kawaguchi, Saitama 332-0012, Japan.

[3] Molecular Cell Engineering Laboratory, National Institute of Genetics, Research Organization of Information and Systems (ROIS), and Department of Genetics, SOKENDAI (The Graduate University of Advanced Studies), Yata 1111, Mishima, Shizuoka 411-8540, Japan.

* Corresponding author:
E-mail: kiyomitsu@bio.nagoya-u.ac.jp
Phone & Fax: +81-52-788-6174
Characters: 29,170 characters

Abstract

During spindle assembly, microtubules are spatially organized by the chromosome-derived Ran-GTP gradient. Previous work demonstrated that Ran-GTP releases spindle assembly factors such as HURP from inhibitory importins to assemble microtubules near chromosomes. However, the significance and mechanisms of Ran-mediated spindle assembly remains poorly understood, especially in somatic cells. Here, we systematically depleted RCC1 (Ran-GEF), RanGAP1, and importin-β in human cells using auxin-inducible degron technology. We demonstrate that depletion of RCC1, but not RanGAP1, causes short metaphase spindles that lack HURP on kinetochore-fibers (k-fibers). Surprisingly, we find that importin-β co-localizes with HURP to k-fibers, where it acts as an active, not inhibitory, regulator for HURP. HURP and importin-β are mutually dependent for their k-fiber localization and coordinately regulated by Ran-GTP. In addition, importin-β mutants lacking Ran-GTP binding fail to accumulate on k-fibers. Together, we propose a model in which, in the presence of microtubules, importin-β still interacts with HURP following Ran-GTP binding and further promotes HURP's microtubule association to stabilize k-fibers.

(160 words)

Introduction

The spindle is a universal microtubule-based macromolecular structure that plays crucial roles for accurate cell division in eukaryotes (McIntosh and Hays, 2016). The spatial organization of microtubules and microtubule-associated proteins is crucial for the proper assembly and function of the spindle in both mitosis and meiosis (Bennabi et al., 2016; Heald and Khodjakov, 2015). During animal mitosis, both chromosome- and centrosome-derived signals organize the mitotic spindle structure by spatially regulating microtubule nucleation, polymerization/depolymerization, transport, sliding, and cross-linking (Goshima and Scholey, 2010; Petry, 2016; Walczak and Heald, 2008). During female meiosis, chromosome-derived signals play particularly dominant roles in spindle assembly as centrosomes are absent (Beaven et al., 2017; Bennabi et al., 2016; Mogessie et al., 2018).

Chromosome-derived signals consist of two distinct pathways - the Ran-GTP gradient and chromosome passenger complex (CPC)-based signals (Zierhut and Funabiki, 2015). Pioneering work using meiotic *Xenopus* egg extracts established a model in which a chromosome-derived Ran-GTP gradient promotes spindle assembly by activating spindle assembly factors (SAFs) such as NuMA and TPX2 by releasing them from inhibitory importin proteins in the vicinity of chromosomes (Fig.1A) (Kalab and Heald, 2008; Nachury et al., 2001; Wiese et al., 2001). At present, several microtubule-binding proteins, such as HURP (Forbes et al., 2015; Sillje et al., 2006), have been identified as spindle assembly factors that promote spindle assembly downstream of Ran-GTP gradient (Forbes et al., 2015). In parallel, chromatin-bound CPC promotes microtubule polymerization around chromosomes by locally inhibiting

65 microtubule-destabilizing factors such as MCAK and Op18 (Kelly et al., 2007; Maresca
66 et al., 2009; Sampath et al., 2004).

67 The Ran-GTP gradient is generated by two spatially-separated opposing
68 enzymes. Regulator of chromosome condensation 1 (RCC1), is a guanine nucleotide
69 exchange factor (GEF) for Ran (Bischoff and Ponstingl, 1991) and localizes to
70 chromosomes to convert the small GTPase Ran from its GDP- to GTP-bound form. In
71 contrast, RanGAP1, a GTPase-activating protein (GAP) for Ran, predominantly
72 localizes to the cytoplasm to promote Ran's intrinsic GTPase activity (Bischoff et al.,
73 1994) (Fig. 1A). The Ran-GTP gradient has been best characterized in meiotic *Xenopus*
74 egg extracts, but is also found in other meiotic and mitotic cell types (Dumont et al.,
75 2007; Kalab et al., 2006; Moutinho-Pereira et al., 2013). In addition to a role in spindle
76 assembly, we previously demonstrated that the Ran-GTP gradient promotes spindle
77 positioning by controlling the spatial organization of cortical complexes in somatic
78 human cells (Kiyomitsu and Cheeseman, 2012; Kiyomitsu and Cheeseman, 2013).
79 Although the Ran-GTP gradient is conserved and critical for meiotic spindle assembly
80 (Dumont et al., 2007; Holubcova et al., 2015), its significance for mitotic spindle
81 assembly has been debated and appears to vary across cell types (Furuta et al., 2016;
82 Hasegawa et al., 2013; Moutinho-Pereira et al., 2013).

83 To understand the significance and mechanisms of Ran-mediated spindle
84 assembly in human mitotic cells, we sought to systematically deplete and visualize
85 endogenous Ran-associated proteins in living cells by combining auxin-inducible degron
86 (AID) technology and CRISPR/Cas9-mediated genome editing (Natsume et al., 2016).
87 We found that degradation of RCC1 causes short mitotic spindle and disrupts the

spatial localization of HURP in human cells. Unexpectedly, we found that importin-β depletion caused mitotic phenotypes similar to RCC1 depletion, but not RanGAP1 depletion, which is opposite to what is predicted based on prevailing models (Fig. 1A). Importantly, we demonstrate that importin-β co-localizes with HURP to k-fibers downstream of RCC1 and that importin-β enriches HURP on k-fibers in coordination with Ran-GTP gradient. Based on our findings, we propose a revised model that, in the presence of microtubules, importin-β is still able to interact with HURP following Ran-GTP-binding and positively regulates HURP's k-fiber localization in coordination with Ran-GTP to promote functional k-fiber assembly.

Results

Auxin-inducible degradation of RCC1 causes short spindle in human cells

To understand the molecular mechanisms of Ran-GTP-dependent spindle assembly in mitotic human cells, we sought to systematically deplete Ran-associated proteins using auxin-inducible degron (AID) technology (Fig. 1A, B) (Natsume et al., 2016). We first targeted RCC1, a Ran-GEF, which should deplete the GTP-bound form of Ran. We introduced a C-terminal mAID-mClover (mAC) tag into both alleles of the RCC1 genomic locus (Fig. 1C and Fig. S1A) in parental tet-OsTIR1 HCT116 cells that conditionally express OsTIR1 following the addition of doxycycline (Dox) (Fig.1B) (Natsume et al., 2016). To visualize NuMA, a spindle assembly factors regulated by Ran (Chang et al., 2017; Nachury et al., 2001; Wiese et al., 2001), we further integrated mCherry into both alleles of the NuMA genomic locus (Fig. 1C and S1B). This double knock-in cell line grew normally, and both RCC1-mAC and NuMA-mCherry displayed their expected localization patterns (Fig. 1D, E). This suggests that these fusion constructs did not affect the functions of endogenous RCC1 and NuMA.

To analyze the functions of RCC1, we performed time-lapse imaging of RCC1-depleted cells following treatment with Dox and auxin (IAA). After 18-24 hrs, the fluorescence intensity of RCC1-mAC was reduced to undetectable levels (Fig. 1D-F), although some populations of cells still displayed RCC1-mAC signals possibly due to heterogeneous induction of OsTIR1 (Fig. 1F, 2nd panels). RCC1-depleted cells progressed through mitosis, but nuclear shape was severely impaired following mitotic exit (Fig. 1F, t=1:00). This is consistent with the phenotypes observed in RCC1-depleted chicken DT40 cells (Furuta et al., 2016). NuMA did not localize to these abnormal nuclei

(Fig. 1F, t=1:00), whereas NuMA still localized to the nucleus prior to mitosis even in the absence of RCC1 (Fig. 1F, t= - 0:10). This suggests that NuMA is maintained in the nucleus once imported. Importantly, metaphase spindle length became shorter in RCC1-depleted cells (Fig. 1D, G). In addition, mitotic duration from nuclear envelope breakdown (NEBD) to anaphase onset was slightly but significantly delayed (Fig. 1F, H). However, the spindle localization of NuMA was virtually unaffected following RCC1 depletion (Fig. 1D-F). These results suggest that RCC1 is required for proper spindle assembly and mitotic progression in human HCT116 cells, probably by activating the functions of spindle assembly factors distinct from NuMA.

RanGAP1 is dispensable for mitotic spindle assembly

To analyze the functional contributions of the Ran-GTP gradient during mitosis, we next sought to increase Ran-GTP level by depleting RanGAP1. Endogenously tagged RanGAP1 (RanGAP1-mAC) localized to the cytoplasm and was excluded from chromosomes (Fig. 2A-B, S1C-D), but was also weakly detectable at kinetochores in metaphase, consistent with prior work (Joseph et al., 2002). However, degradation of RanGAP1 did not cause a clear phenotype during mitosis (Fig. 2B-D, Fig. S1E-F): the bipolar spindle assembled normally, and metaphase spindle length and mitotic duration in RanGAP1-depleted cells were almost identical to those in control cells. These results suggest that RanGAP1-mediated hydrolysis of Ran-GTP is dispensable for mitotic spindle assembly in HCT116 cells.

Degradation of importin-β causes mitotic phenotypes similar to RCC1, but not RanGAP1 depletion

In the current model, Ran-GTP activates spindle assembly factors by releasing them from inhibitory importins in the vicinity of chromosomes (Fig. 1A). Based on this model, depletion of importin-β would liberate spindle assembly factors throughout the cell resulting in mitotic phenotypes similar to Ran-GAP1 depletion. To test this, we next depleted endogenous importin-β by fusing it with mAID-mClover (mAC) (Fig. 2E, F and Fig. S2A-B). Unexpectedly, we found that endogenous importin-β-mAC accumulated at the chromosome-proximal region of bundled kinetochore-microtubules (k-fibers) in living cells (Fig. 2F top, S2C). This contrasts with a previous study that found importin-β localizes to spindle poles in pre-extracted fixed cells (Ciciarello et al., 2004). The k-fiber localization of importin-β was not an artifact of mAC tagging, as it was observed after immunostaining of endogenous importin-β without tags (Fig. S2D). Importantly, importin-β depletion resulted in a defective spindle structure characterized by short mitotic spindles and delayed mitotic progression (Fig. 2G-J), although NuMA's localization was almost normal (Fig. 2F, H). This phenotype is similar to RCC1 depletion, but not RanGAP1 depletion. These results suggest that, in contrast to prevailing models (Fig. 1A), importin-β promotes spindle assembly, but does not inhibit this process.

RCC1 and importin-β are required for HURP localization to k-fibers

The phenotypic similarity between importin-β and RCC1 depletions was not readily explainable by the current model in which Ran activates spindle assembly factors by releasing inhibitory importins (Fig. 1A). Rather, it could be interpreted that importin-β

positively regulates spindle assembly factors downstream of RCC1 to promote spindle assembly. To test this possibility, we next analyzed the localization of importin-β and known spindle assembly factors including NuMA, TPX2 (Gruss et al., 2001), and HURP (Sillje et al., 2006). Strikingly, RCC1 depletion abolished k-fiber accumulation of both importin-β (Fig. 3A, Fig. S2E) and HURP(Fig. 3B, Fig. S2F). HURP localized diffusely in the cytoplasm with weak accumulation at spindle poles in RCC1-depleted cells (Fig. 3B). In contrast, the spindle localization of NuMA (Fig. 1D) and TPX2 was virtually unaffected in RCC1-depleted cells (Fig. 3C and S2G).

We next analyzed HURP localization in importin-β-depleted cells. In control cells, importin-β co-localized with SNAP-tagged endogenous HURP (HURP-SNAP) to k-fibers (Fig. 3D top, S2H). However, importin-β depletion abolished the k-fiber localization of HURP, resulting in strong accumulation of HURP at spindle poles of the short spindle (Fig. 3D bottom, Fig. S2I). These results suggest that HURP is a key downstream target of importin-β in human HCT116 cells.

HURP is required to target importin-β to k-fibers and control proper metaphase spindle length

Previous work demonstrated that importin-β directly interacts with HURP (Sillje et al., 2006). However, it was assumed that importin-β dissociates from HURP following the binding of Ran-GTP to importin-β (Fig. 1A) (Sillje et al., 2006). To understand the relationship between importin-β and HURP for their k-fiber localization and function, we next targeted endogenous HURP by introducing a mAID-mClover-3xFLAG (mACF) tag (Fig. 4A, Fig. S3A). In control cells, HURP-mACF co-localized with endogenous

mCherry-tagged importin-β (importin-β-mCh) on k-fibers (Fig. 4B top, Fig. S3B). However, HURP depletion resulted in diminished importin-β to k-fibers (Fig. 4B, bottom, 4C) and reduced mitotic spindle length (Fig. 4D) as observed for importin-β depleted cells (Fig. 2I). These results suggest that HURP localizes to k-fiber along with importin-β, likely by maintaining the interaction with importin-β.

Ran-GTP promotes spindle microtubule enrichment of HURP and importin-β.

In contrast to prior expectations, our results suggest that importin-β acts positively to target HURP to k-fibers following Ran-GTP binding instead of dissociating from HURP. To probe this model, we next analyzed the behaviors of importin-β and HURP in RanGAP1-depleted cells in which Ran-GTP levels are expected to be increased. Intriguingly, following the depletion of RanGAP1, both importin-β and HURP localized to k-fibers, but additionally accumulated on spindle microtubules with increased intensities (Fig. 5A-B, Fig. S1D). This suggests that importin-β and HURP behave together and interact with microtubules more stably in response to Ran-GTP.

Ran-GTP binding to importin-β is required for k-fiber localization of importin-β

Ran-GTP directly binds to importin-β, resulting in cargo release from importin-β (Fig.1A) (Lee et al., 2005; Zachariae and Grubmuller, 2008). However, our results indicate that importin-β still interacts with HURP following Ran-GTP binding and localizes to k-fibers together with HURP and Ran-GTP. To test this model, we next sought to analyze whether Ran-GTP localizes to k-fibers. To visualize Ran-GTP, we expressed a

211 constitutively active mutant of Ran, RanQ69L, that is unable to hydrolyze bound GTP
212 (Bischoff et al., 1994) and thus expected to be as GTP-bond form. Consistent with our
213 model, ectopically-expressed mCherry-tagged RanQ69L was detected on k-fibers (25 %,
214 n=68, Fig. 5C and Fig. S4A) in HEK293 cells. In contrast, a dominant negative mutant
215 that is unable to bind to GTP, mCh-RanT24N, predominantly localized to chromosomes
216 (100%, n=30) (Fig. 5C) (Kiyomitsu and Cheeseman, 2012) and was never detected on
217 k-fibers.

218 We next analyzed whether Ran-GTP binding to importin-β is required for the k-
219 fiber localization of importin-β. For this, we analyzed the localization of importin-β ΔN10
220 and ΔN70 mutants that are compromised or completely unable to bind Ran-GTP,
221 respectively (Chi et al., 1997; Kutay et al., 1997), but are still able to interact with HURP
222 (Song and Rape, 2010). Transiently expressed mCherry-tagged wild type (WT)
223 importin-β displayed k-fiber-like localization in ~40 % of HEK293 cells (Fig. 5D, n=62).
224 In contrast, both importin-β ΔN10 and ΔN70 mutants failed to localize to k-fibers, but
225 instead accumulated on spindle microtubules or spindle poles (Fig. 5D), probably by
226 binding to its other cargos. These results support our model that importin-β localizes to
227 k-fibers by binding to Ran-GTP.
228

Discussion

Importin-β positively regulates HURP's k-fiber accumulation.

Here, we found that importin-β co-localizes with HURP to k-fibers (Fig. 2F, 3D, 4B, S2D), and positively regulates metaphase spindle length and HURP's k-fiber accumulation (Fig. 2I, 3D) in response to the Ran-GTP gradient (Fig. 3A-B, 5A-B, D). Based on these findings, we propose a revised model in which Ran-GTP binding to HURP-importin-β complexes leads to different outcomes in response to the presence or absence of microtubules (Fig. 6).

Upon Ran-GTP binding, importin-β changes its conformation (Lee et al., 2005), which leads to dissociation of importin-β from HURP in the cytoplasm (Sillje et al., 2006; Song and Rape, 2010) (Fig. 6, Classical model). However, given that HURP's importin-β binding region is located within the second microtubule-binding domain (MBD2) of HURP (Song and Rape, 2010), we hypothesize that, in the presence of microtubules, HURP captures microtubules through its MBD2 domain without releasing Ran-GTP bound importin-β (Fig. 6, New model-I). Since the microtubule-binding domain (MBD1) of HURP constitutively interacts with microtubules even in the presence of importin-β (Song et al., 2014), a HURP-importin-β-Ran-GTP ternary complex may bundle k-fibers by linking different microtubules using two microtubule-binding domains (MBD1 and 2) of HURP (Fig. 6, New model-I). This model is consistent with previous in vitro studies reported by Sillje et al. (Sillje et al., 2006) in which purified microtubules were mixed with recombinant HURP, importin-β and RanQ69L. Whereas importin-β addition to HURP and microtubules largely suppressed HURP's microtubule bundling activity, simultaneous addition of importin-β and RanQ69L resulted in HURP that still displayed

mild microtubule bundling (see Figure 7b in (Sillje et al., 2006)), suggesting that Ran-GTP suppresses importin-β's inhibitory activity in the presence of microtubules. The Ran-GTP dependent activation of HURP-importin-β complexes may be suitable for bundling short microtubules nucleated around kinetochores to form stable k-fibers (Sikirzhytski et al., 2018).

Importin-β has dual functions in response to the Ran-GTP gradient to amplify HURP's k-fiber accumulation

Although HURP has microtubule-binding activities, we demonstrate that HURP itself is unable to localize to k-fibers in the absence of importin-β, and instead accumulates on spindle microtubules around spindle poles (Fig. 3D). This indicates that importin-β functions not only to enrich HURP on k-fibers, but also to exclude HURP from spindle microtubules around the spindle poles. We propose that importin-β increases the microtubule-binding affinity of HURP by exposing its MBD2 domain following Ran-GTP binding around chromosomes (Fig. 6, New model-I), and decreases HURP's microtubule binding activity by masking MBD2 around the spindle poles (Fig. 6, New model-II). Thus, importin-β can act either positively or negatively in response to the Ran-GTP gradient to synergistically enrich HURP on k-fibers near chromosomes.

K-fiber accumulation of HURP-importin-β complexes is required for proper metaphase spindle formation

We found that degradation of either RCC1, importin-β, or HURP, but not RanGAP1, caused short metaphase spindles in human HCT116 cells (Fig. 1G, 2C, 2I, S2I, 4D). Because HURP is required for the stabilization of k-fibers (Sillje et al., 2006) and the generation or maintenance of spindle microtubules (Uehara and Goshima, 2010), loss of k-fiber accumulation of HURP would lead to destabilization of k-fibers and/or spindle microtubules resulting in short metaphase spindles. In contrast, NuMA and TPX2 accumulate around spindle poles even in the absence of RCC1 (Fig. 1D, 3C). Given the severe defects in bipolar spindle assembly following NuMA or TPX2 depletion (Garrett et al., 2002; Hueschen et al., 2017; Okumura et al., 2018), NuMA and TPX2 would be able to function independently of Ran-GTP in HCT116 cells. In fact, co-depletion of RCC1 and NuMA caused severe mitotic phenotypes (T.K. unpublished observation). Other Ran-GTP independent mechanisms may exist to liberate these spindle assembly factors from importins in mitotic cells. In addition, other mechanisms such as CPC-dependent spindle assembly (Kelly et al., 2007; Maresca et al., 2009; Sampath et al., 2004) and TACC3/chTOG/clathrin complex-mediated k-fiber stabilization (Booth et al., 2011) may play dominant roles to assemble a functional spindle in mitotic cells. In contrast to mitosis, Ran pathway plays critical roles for spindle assembly in female meiosis (Dumont et al., 2007; Holubcova et al., 2015). It will be interesting to test whether our model (Fig. 6) is conserved in meiosis.

Acknowledgments

We thank I. M. Cheeseman for critical reading of the manuscript, R. Inaba, and K. Murase for technical assistance. This work was supported by grants from PRESTO program (JPMJPR13A3) of the Japan Science and Technology agency (JST) for T.K, a Career Development Award of the Human Frontier Science Program (CDA00057/2014-C) for T.K., KAKENHI (16K14721 and 17H05002 for T.K, 17H01431 for G.G.) of the Japan Society for Promotion of Science (JSPS), Collaborative Research Program (2014-B, 2015-A1, 2016-A1 for T.K and M.K) of the National Institute of Genetics (NIG), and the Naito Foundation for T.K.

Author contributions

Conceptualization, T.K. ; Investigation, K.T., H.H., M.N., M.O, and T.K. ; Formal analysis, K.T., and T.K. ; Methodology, T.K. and M.K. ; Writing, T.K. and G.G. ; Supervision, T.K. and G.G. ; Funding Acquisition, T.K., M.K. and G.G.

Declaration of interests

The authors declare no competing interests.

Materials and methods

- Plasmid Construction

Plasmids for CRISPR/Cas9-mediated genome editing and auxin-inducible degron were constructed according to the protocol described in Natsume et al., (Natsume et al., 2016) and Okumura et al., (Okumura et al., 2018). To construct donor plasmids containing homology arms for RCC1 (~500-bp homology arms), RanGAP1 (~500-bp arms), importin-β (~500-bp homology arms), HURP (~200-bp homology arms), and TPX2 (~200-bp homology arms), gene synthesis services from Eurofins Genomics K.K. (Tokyo, Japan) or Genewiz (South Plainsfield, NJ) were used for RCC1 and others, respectively. To express mCherry-tagged Ran or importin-β mutants, the cDNA sequences were inserted into plasmid pIC194 (#44433, Addgene)(Kiyomitsu and Cheeseman, 2012), which contains a 61 amino acid linker between mCherry and the coding sequence. Plasmids and sgRNA sequences used in this study are listed in Supplementary Tables S1 and S2, and will be deposited to Addgene.

- Cell Culture, Cell Line Generation and Antibodies

HCT116 cells and Flip-in TRex 293 cells were cultured as described previously (Kiyomitsu et al., 2011; Okumura et al., 2018). Knock-in cell lines for HCT116 cells or Flip-In TRex 293 cells were generated according to the procedures described in Okumura et al., (Okumura et al., 2018) or Kiyomitsu et al., (Kiyomitsu et al., 2011), respectively. To activate the auxin-inducible degradation, cells were treated with 2 μg/mL Dox and 500 μM indoleacetic acid (IAA) for 20–24 h. Cells with undetectable mClover signals were analyzed. To expresss mCherry-tagged Ran mutants in Fig. 5C, cells were incubated with 1 μg/mL tetracycline (MP biomedicals) for >18 h. The cell lines and primers used in this study are listed in Tables S1 and S3, respectively.

Antibodies against tubulin (DM1A, Sigma-Aldrich, 1:2,000), NuMA (Abcam, 1:1,000), RCC1 (Cell Signaling Technology, D15H6, Rabbit mAb, 1:100), RanGAP1 (Santa Cruz Biotechnology, H-180, 1:200), importin-β (GeneTex, 3E9 Mouse mAb, 1:100), and HURP (E. Nigg laboratory, 1 : 200) were used for western blotting. For RCC1 immunoblots, the membrane was incubated with the anti-RCC1 antibody overnight at 4 °C.

- Microscope System

Imaging was performed using spinning-disc confocal microscopy with a 60× 1.40 numerical aperture objective lens (Plan Apo λ, Nikon, Tokyo, Japan). A CSU-W1 confocal unit (Yokogawa Electric Corporation, Tokyo, Japan) with three lasers (488, 561, and 640 nm, Coherent, Santa Clara, CA) and an ORCA-Flash4.0 digital CMOS camera (Hamamatsu Photonics, Hamamatsu City, Japan) were attached to an ECLIPSE Ti-E inverted microscope (Nikon) with a perfect focus system. DNA images were obtained using SOLA LED light engine (Lumencor, Beaverton, OR) and appropriate filters. A stage-top incubator (Tokai Hit, Fujinomiya, Japan) was used to maintain the same conditions used for cell culture (37 °C and 5% CO_2).

- Immunofluorescence and Live Cell Imaging

For immunofluorescence in Figure S2D, HURP-mACF cells were fixed with PBS

containing 3% paraformaldehyde and 2% sucrose for 10 min at room temperature. Fixed cells were permeabilized with 0.5% Triton X-100™ for 5 min on ice, and pretreated with PBS containing 1% BSA for 10 min at room temperature after washing with PBS. Importin-β was visualized using the anti-importin-β antibody (1:500). Images of multiple z-sections were acquired by spinning-disc confocal microscopy using 0.5-μm spacing and camera binning 2. Maximally projected images from 3 z-sections were shown.

For time-lapse imaging in Fig. 1E-F, S1E-F and Fig. 2G-H, cells were cultured on glass-bottomed dishes (CELLview™, #627870, Greiner Bio-One, Kremsmünster, Austria) and maintained in a stage-top incubator (Tokai Hit) to maintain the same conditions used for cell culture (37 °C and 5% CO_2). Two z-section images using 1.0-μm spacing were acquired with camera binning 2 and maximally projected z-stack images were shown. In other live cell imaging, three to five z-section images using 0.5-μm spacing were acquired and single z-section images were shown, unless otherwise specified. Microtubules was stained with 50 nM SiR-tubulin (Spirochrome) for >1 h prior to image acquisition. DNA was stained 50 ng/mL Hoechst® 33342 (Sigma-Aldrich) for > 1 h before observation. To visualize SNAP-tagged HURP in Fig. 3D, cells were incubated with 0.1 μM TMR-STAR (New England BioLabs) for > 2 h, and those chemical probes were removed before observation. To optimize image brightness, same linear adjustments were applied using Fiji and Photoshop.

- Statistical Analysis

To determine the significance of differences between the mean values obtained for two experimental conditions, Welch's *t*-tests (Prism 6; GraphPad Software, La Jolla, CA) or a Z-test for proportions (Allto Consulting, Leeds, UK) were used as indicated in the figure legends.

388 **Table S1: Cell lines used in this study.**

No.	Name	Description	Clone No.	Plasmids used	Parental cell	Reference
1	HCT116 tet-OsTIR1	AAVS1::PTRE3G OsTIR1 (Puro)		pAAVS1 T2 and MK243 (Addgene#72835)		(Natsume et al., 2016)
2	RCC1-mAC	AAVS1::PTRE3G OsTIR1 (Puro), RCC1:: RCC1-mAID-mClover (Neo)	1	pTK361+ pHH45	1	This study
3	RCC1-mAC + NuMA-mCh	AAVS1::PTRE3G OsTIR1 (Puro), RCC1:: RCC1-mAID-mClover (Neo), NuMA1:: NuMA-mCh (Hygro)	1	pTK372+ pTK435	2	This study
4	RanGAP1-mAC	AAVS1::PTRE3G OsTIR1 (Puro), RanGAP1:: RanGAP1-mAID-mClover (Neo)	9	pHH49 + pHH51	1	This study
5	RanGAP1-mAC + NuMA-mCh	AAVS1::PTRE3G OsTIR1 (Puro), RanGAP1:: RanGAP1-mAID-mClover (Neo), NuMA1:: NuMA-mCh (Hygro)	5	pTK372+ pTK435	4	This study
6	importin-β-mAC	AAVS1::PTRE3G OsTIR1 (Puro), importin-β:: importin-β-mAID-mClover (Neo)	7	pHH50 + pHH57	1	This study
7	importin-β-mAC + NuMA-mCh	AAVS1::PTRE3G OsTIR1 (Puro), importin-β:: importin-β-mAID-mClover (Neo), NuMA1:: NuMA-mCh (Hygro)	1	pTK372+ pTK435	6	This study
8	RCC1-mAC + importin-β-mCh	AAVS1::PTRE3G OsTIR1 (Puro), RCC1:: RCC1-mAID-mClover (Neo), NuMA1:: NuMA-mCh (Hygro)	6	pHH50 +pTK481	2	This study
9	RCC1-mAC + HURP-mCh	AAVS1::PTRE3G OsTIR1 (Puro), RCC1:: RCC1-mAID-mClover (Neo), HURP:: HURP-mCh (Hygro)	8	pTK532+ pTK541	2	This study
10	RCC1-mAC + TPX2-mCh	AAVS1::PTRE3G OsTIR1 (Puro), RCC1:: RCC1-mAID-mClover (Neo), TPX2:: TPX2-mCh (Hygro)	1	pTK527+ pTK502	2	This study
11	RanGAP1-mAC + HURP-mCh	AAVS1::PTRE3G OsTIR1 (Puro), RanGAP1:: RanGAP1-mAID-mClover (Neo), HURP:: HURP-mCh (Hygro)	5	pTK532+ pTK541	4	This study
12	RanGAP1-mAC + importin-β-mCh	AAVS1::PTRE3G OsTIR1 (Puro), RanGAP1:: RanGAP1-mAID-mClover (Neo), importin-β:: importin-β-mCh (Hygro)	12	pHH50 +pTK481	4	This study
13	importin-β-mAC + HURP-SNAP	AAVS1::PTRE3G OsTIR1 (Puro), importin-β:: importin-β-mAID-mClover (Neo), HURP:: HURP-SNAP (Hygro)	3	pTK532+ pTK589	6	This study
14	HURP-mACF	AAVS1::PTRE3G OsTIR1 (Puro), HURP:: HURP-mAID-mClover-3FLAG (Neo)	13	pTK532+ pTK596	1	This study
15	HURP-mACF + importin-β-mCh	AAVS1::PTRE3G OsTIR1 (Puro), HURP:: HURP-mAID-mClover-3FLAG (Neo), importin-β:: importin-β-mCh (Hygro)	14	pHH50 +pTK481	14	This study
16	HEK293 Flip-In TRex					(Kiyomitsu et al., 2011)
17	HEK293 Flip-In TRex + mCh-RanT24N	Flip-In:: mCh-RanT24N (Hygro)	1	pTK285+ pOG44	16	This study
18	HEK293 Flip-In TRex + mCh-RanQ69L	Flip-In:: mCh-RanQ69L (Hygro)	1	pTK286+ pOG44	16	This study

389 **Table S2: sgRNA sequences for CRISPR/Cas9-mediated genome editing**

Gene locus	sgRNA (5'-3')	PAM	Plasmid Name
NuMA1 (C-terminus)	gtggggccactcactggtac	tgg	pTK372 (Okumura et al., 2018)
RCC1 (C-terminus)	gactgtatgctggcccccgc	tgg	pTK361
RanGAP1 (C-terminus)	tctgctgcagacgctgtaca	agg	pHH49
importin-β (C-terminus)	agttcgagccgccgcccgaa	agg	pHH50
HURP	caaaattctcctggttgtag	agg	pTK532
TPX2	tgcggataccgcccggcaat	ggg	pTK527

390

391 **Table S3: PCR primers to confirm gene editing**

Gene	Primer sequence	Primer name	Figures
RCC1	gaatgccattccaggcag	oHH88	Figure S1A
RCC1	ttctgcacgttcctctgg	oHH89	Figure S1A
NUMA1	gagcctcaaagaaggccc	oTK542	Figure S1B, S1D, S2B
NUMA1	agcaggaaccagggcctac	oTK566	Figure S1B, S1D, S2B
RanGAP1	gctgccgcaggaccagggcttggtg	oHH93	Figure S1C
RanGAP1	attccctggcctatgtctgctggaa	oHH94	Figure S1C
HURP	ctcttgatggatactttactg	oTK749	Figure S1D, S2F, S2H, S3A
HURP	cccttgagaaagagtatatcta	oTK750	Figure S1D, S2F, S2H, S3A
importin-β	ggagtaaggagttttgagagtatcg	oHH97	Figure S1D, S2A, S2E, S3B
importin-β	aaatcttctctagagctaggcaacg	oHH98	Figure S1D, S2A, S2E, S3B
TPX2	tctgacatccctctcactg	oTK660	Figure S2G
TPX2	ggagtctaatcgagacattc	oTK661	Figure S2G

392

393

References

Beaven, R., R.N. Bastos, C. Spanos, P. Rome, C.F. Cullen, J. Rappsilber, R. Giet, G. Goshima, and H. Ohkura. 2017. 14-3-3 regulation of Ncd reveals a new mechanism for targeting proteins to the spindle in oocytes. *J Cell Biol*. 216:3029-3039.

Bennabi, I., M.E. Terret, and M.H. Verlhac. 2016. Meiotic spindle assembly and chromosome segregation in oocytes. *J Cell Biol*. 215:611-619.

Bischoff, F.R., C. Klebe, J. Kretschmer, A. Wittinghofer, and H. Ponstingl. 1994. RanGAP1 induces GTPase activity of nuclear Ras-related Ran. *Proc Natl Acad Sci U S A*. 91:2587-2591.

Bischoff, F.R., and H. Ponstingl. 1991. Catalysis of guanine nucleotide exchange on Ran by the mitotic regulator RCC1. *Nature*. 354:80-82.

Booth, D.G., F.E. Hood, I.A. Prior, and S.J. Royle. 2011. A TACC3/ch-TOG/clathrin complex stabilises kinetochore fibres by inter-microtubule bridging. *EMBO J*. 30:906-919.

Chang, C.C., T.L. Huang, Y. Shimamoto, S.Y. Tsai, and K.C. Hsia. 2017. Regulation of mitotic spindle assembly factor NuMA by Importin-beta. *J Cell Biol*. 216:3453-3462.

Chi, N.C., E.J. Adam, and S.A. Adam. 1997. Different binding domains for Ran-GTP and Ran-GDP/RanBP1 on nuclear import factor p97. *J Biol Chem*. 272:6818-6822.

Ciciarello, M., R. Mangiacasale, C. Thibier, G. Guarguaglini, E. Marchetti, B. Di Fiore, and P. Lavia. 2004. Importin beta is transported to spindle poles during mitosis and regulates Ran-dependent spindle assembly factors in mammalian cells. *J Cell Sci*. 117:6511-6522.

Dumont, J., S. Petri, F. Pellegrin, M.E. Terret, M.T. Bohnsack, P. Rassinier, V. Georget, P. Kalab, O.J. Gruss, and M.H. Verlhac. 2007. A centriole- and RanGTP-independent spindle assembly pathway in meiosis I of vertebrate oocytes. *J Cell Biol*. 176:295-305.

Forbes, D.J., A. Travesa, M.S. Nord, and C. Bernis. 2015. Reprint of "Nuclear transport factors: global regulation of mitosis". *Curr Opin Cell Biol*. 34:122-134.

Furuta, M., T. Hori, and T. Fukagawa. 2016. Chromatin binding of RCC1 during mitosis is important for its nuclear localization in interphase. *Mol Biol Cell*. 27:371-381.

Garrett, S., K. Auer, D.A. Compton, and T.M. Kapoor. 2002. hTPX2 is required for normal spindle morphology and centrosome integrity during vertebrate cell division. *Curr Biol*. 12:2055-2059.

Goshima, G., and J.M. Scholey. 2010. Control of mitotic spindle length. *Annu Rev Cell Dev Biol*. 26:21-57.

Gruss, O.J., R.E. Carazo-Salas, C.A. Schatz, G. Guarguaglini, J. Kast, M. Wilm, N. Le Bot, I. Vernos, E. Karsenti, and I.W. Mattaj. 2001. Ran induces spindle assembly by reversing the inhibitory effect of importin alpha on TPX2 activity. *Cell*. 104:83-93.

Hasegawa, K., S.J. Ryu, and P. Kalab. 2013. Chromosomal gain promotes formation of a steep RanGTP gradient that drives mitosis in aneuploid cells. *J Cell Biol*. 200:151-161.

Heald, R., and A. Khodjakov. 2015. Thirty years of search and capture: The complex simplicity of mitotic spindle assembly. *J Cell Biol*. 211:1103-1111.

Holubcova, Z., M. Blayney, K. Elder, and M. Schuh. 2015. Human oocytes. Error-prone chromosome-mediated spindle assembly favors chromosome segregation defects in human oocytes. *Science*. 348:1143-1147.

Hueschen, C.L., S.J. Kenny, K. Xu, and S. Dumont. 2017. NuMA recruits dynein activity to microtubule minus-ends at mitosis. *Elife*. 6.

Joseph, J., S.H. Tan, T.S. Karpova, J.G. McNally, and M. Dasso. 2002. SUMO-1 targets RanGAP1 to kinetochores and mitotic spindles. *J Cell Biol*. 156:595-602.

Kalab, P., and R. Heald. 2008. The RanGTP gradient - a GPS for the mitotic spindle. *J Cell Sci*. 121:1577-1586.

Kalab, P., A. Pralle, E.Y. Isacoff, R. Heald, and K. Weis. 2006. Analysis of a RanGTP-regulated gradient in mitotic somatic cells. *Nature*. 440:697-701.

Kelly, A.E., S.C. Sampath, T.A. Maniar, E.M. Woo, B.T. Chait, and H. Funabiki. 2007. Chromosomal enrichment and activation of the aurora B pathway are coupled to spatially regulate spindle assembly. *Dev Cell*. 12:31-43.

Kiyomitsu, T., and I.M. Cheeseman. 2012. Chromosome- and spindle-pole-derived signals generate an intrinsic code for spindle position and orientation. *Nat Cell Biol*. 14:311-317.

Kiyomitsu, T., and I.M. Cheeseman. 2013. Cortical dynein and asymmetric membrane elongation coordinately position the spindle in anaphase. *Cell*. 154:391-402.

Kiyomitsu, T., H. Murakami, and M. Yanagida. 2011. Protein interaction domain mapping of human kinetochore protein Blinkin reveals a consensus motif for binding of spindle assembly checkpoint proteins Bub1 and BubR1. *Mol Cell Biol*. 31:998-1011.

Kutay, U., E. Izaurralde, F.R. Bischoff, I.W. Mattaj, and D. Gorlich. 1997. Dominant-negative mutants of importin-beta block multiple pathways of import and export through the nuclear pore complex. *EMBO J*. 16:1153-1163.

Lee, S.J., Y. Matsuura, S.M. Liu, and M. Stewart. 2005. Structural basis for nuclear import complex dissociation by RanGTP. *Nature*. 435:693-696.

Maresca, T.J., A.C. Groen, J.C. Gatlin, R. Ohi, T.J. Mitchison, and E.D. Salmon. 2009. Spindle assembly in the absence of a RanGTP gradient requires localized CPC activity. *Curr Biol*. 19:1210-1215.

McIntosh, J.R., and T. Hays. 2016. A Brief History of Research on Mitotic Mechanisms. *Biology (Basel)*. 5.

Mogessie, B., K. Scheffler, and M. Schuh. 2018. Assembly and Positioning of the Oocyte Meiotic Spindle. *Annu Rev Cell Dev Biol*. 34:381-403.

Moutinho-Pereira, S., N. Stuurman, O. Afonso, M. Hornsveld, P. Aguiar, G. Goshima, R.D. Vale, and H. Maiato. 2013. Genes involved in centrosome-independent mitotic spindle assembly in Drosophila S2 cells. *Proc Natl Acad Sci U S A*. 110:19808-19813.

Nachury, M.V., T.J. Maresca, W.C. Salmon, C.M. Waterman-Storer, R. Heald, and K. Weis. 2001. Importin beta is a mitotic target of the small GTPase Ran in spindle assembly. *Cell*. 104:95-106.

Natsume, T., T. Kiyomitsu, Y. Saga, and M.T. Kanemaki. 2016. Rapid Protein Depletion in Human Cells by Auxin-Inducible Degron Tagging with Short Homology Donors. *Cell Rep*. 15:210-218.

Okumura, M., T. Natsume, M.T. Kanemaki, and T. Kiyomitsu. 2018. Dynein-Dynactin-NuMA clusters generate cortical spindle-pulling forces as a multi-arm ensemble. *Elife*. 7.

Petry, S. 2016. Mechanisms of Mitotic Spindle Assembly. *Annu Rev Biochem*. 85:659-683.

Sampath, S.C., R. Ohi, O. Leismann, A. Salic, A. Pozniakovski, and H. Funabiki. 2004. The chromosomal passenger complex is required for chromatin-induced microtubule stabilization and spindle assembly. *Cell*. 118:187-202.

Sikirzhytski, V., F. Renda, I. Tikhonenko, V. Magidson, B.F. McEwen, and A. Khodjakov. 2018. Microtubules assemble near most kinetochores during early prometaphase in human cells. *J Cell Biol*. 217:2647-2659.

Sillje, H.H., S. Nagel, R. Korner, and E.A. Nigg. 2006. HURP is a Ran-importin beta-regulated protein that stabilizes kinetochore microtubules in the vicinity of chromosomes. *Curr Biol*. 16:731-742.

Song, L., A. Craney, and M. Rape. 2014. Microtubule-dependent regulation of mitotic protein degradation. *Mol Cell*. 53:179-192.

Song, L., and M. Rape. 2010. Regulated degradation of spindle assembly factors by the anaphase-promoting complex. *Mol Cell*. 38:369-382.

Uehara, R., and G. Goshima. 2010. Functional central spindle assembly requires de novo microtubule generation in the interchromosomal region during anaphase. *J Cell Biol*. 191:259-267.

Walczak, C.E., and R. Heald. 2008. Mechanisms of mitotic spindle assembly and function. *Int Rev Cytol*. 265:111-158.

Wiese, C., A. Wilde, M.S. Moore, S.A. Adam, A. Merdes, and Y. Zheng. 2001. Role of importin-beta in coupling Ran to downstream targets in microtubule assembly. *Science*. 291:653-656.

Zachariae, U., and H. Grubmuller. 2008. Importin-beta: structural and dynamic determinants of a molecular spring. *Structure*. 16:906-915.

Zierhut, C., and H. Funabiki. 2015. Nucleosome functions in spindle assembly and nuclear envelope formation. *Bioessays*. 37:1074-1085.

Figure 1

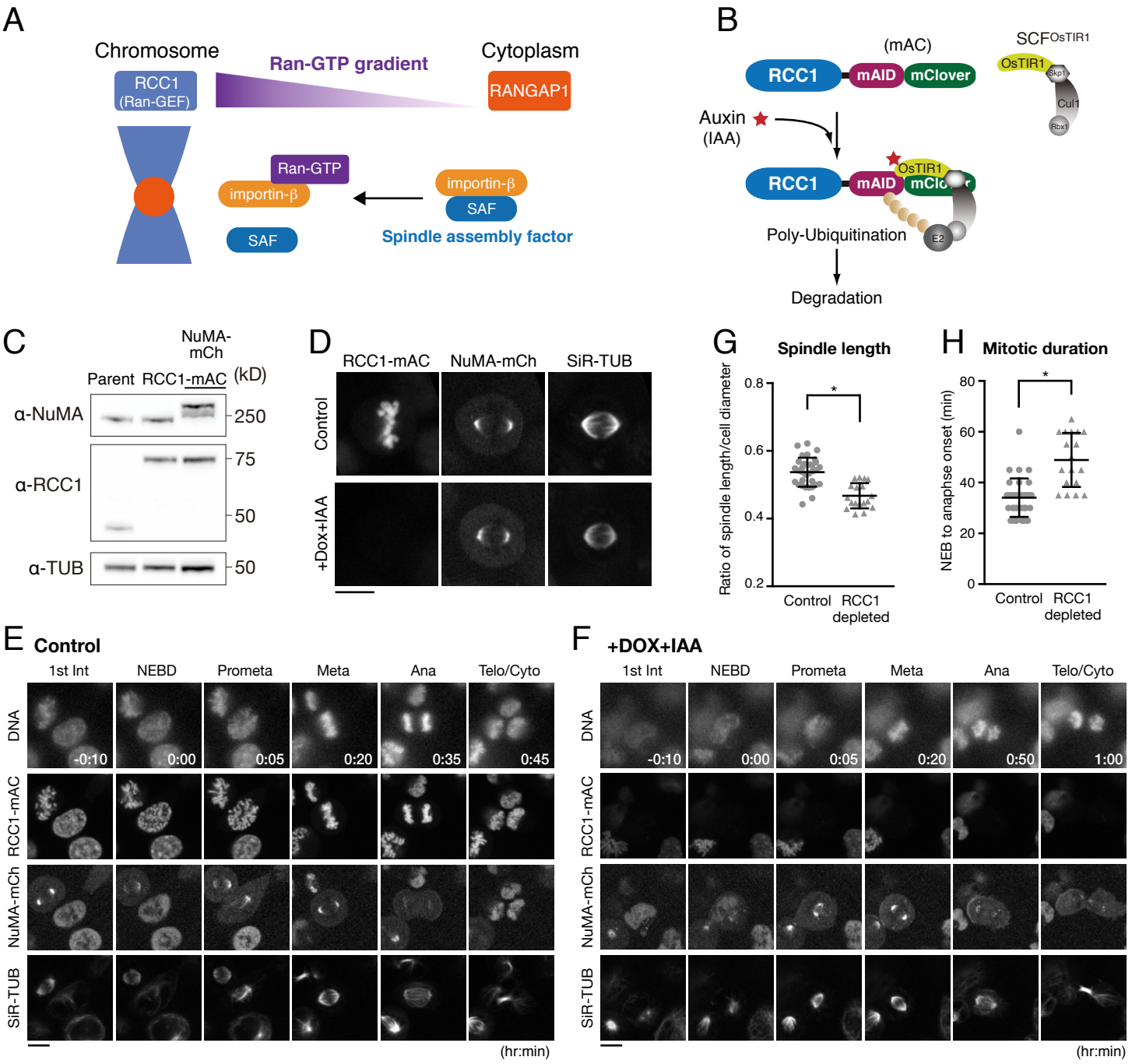

Figure 1. Auxin-inducible degaradation of RCC1 causes short metaphase spindle.

(A) Representation of the mitotic spindle assembly regulated by Ran-related factors. (B) Schematic of the auxin-inducible degradation (AID) system. (C) Immunoblotting for anti-NuMA, anti-RCC1 and anti-α-tubulin (TUB, loading control) showing bi-allelic insertion of the indicated tags. (D) Metaphase RCC1-mAC cells showing live fluorescent images of RCC1-mAC, NuMA-mCherry (mCh), and SiR-tubulin (SiR-TUB) following 24 hrs of Dox and IAA treatment. (E, F) Live fluorescent images of DNA (Hoechst 33342 staining), RCC1-mAC, NuMA-mCh, and SiR-TUB in control (E) and RCC1-depleted (F) cells. (G) Scatterplots of the ratio of spindle length and cell diameter in control (0.54 ± 0.04, n=32) and RCC1-depleted (0.47 ± 0.04, n=23) cells. (H) Scatterplots of mitotic duration (NEBD to anaphase onset) in control (34.1 ± 7.6, n=32) and RCC1-depleted cells (47.2 ± 10.5, n=27). Bars in (G) and (H) indicate mean ± SD from >3 independent experiments. * indicates statistical significance according to Welch's t-test ($p<0.0001$) in (G) and (H). Scale bars = 10 μm.

Figure 2

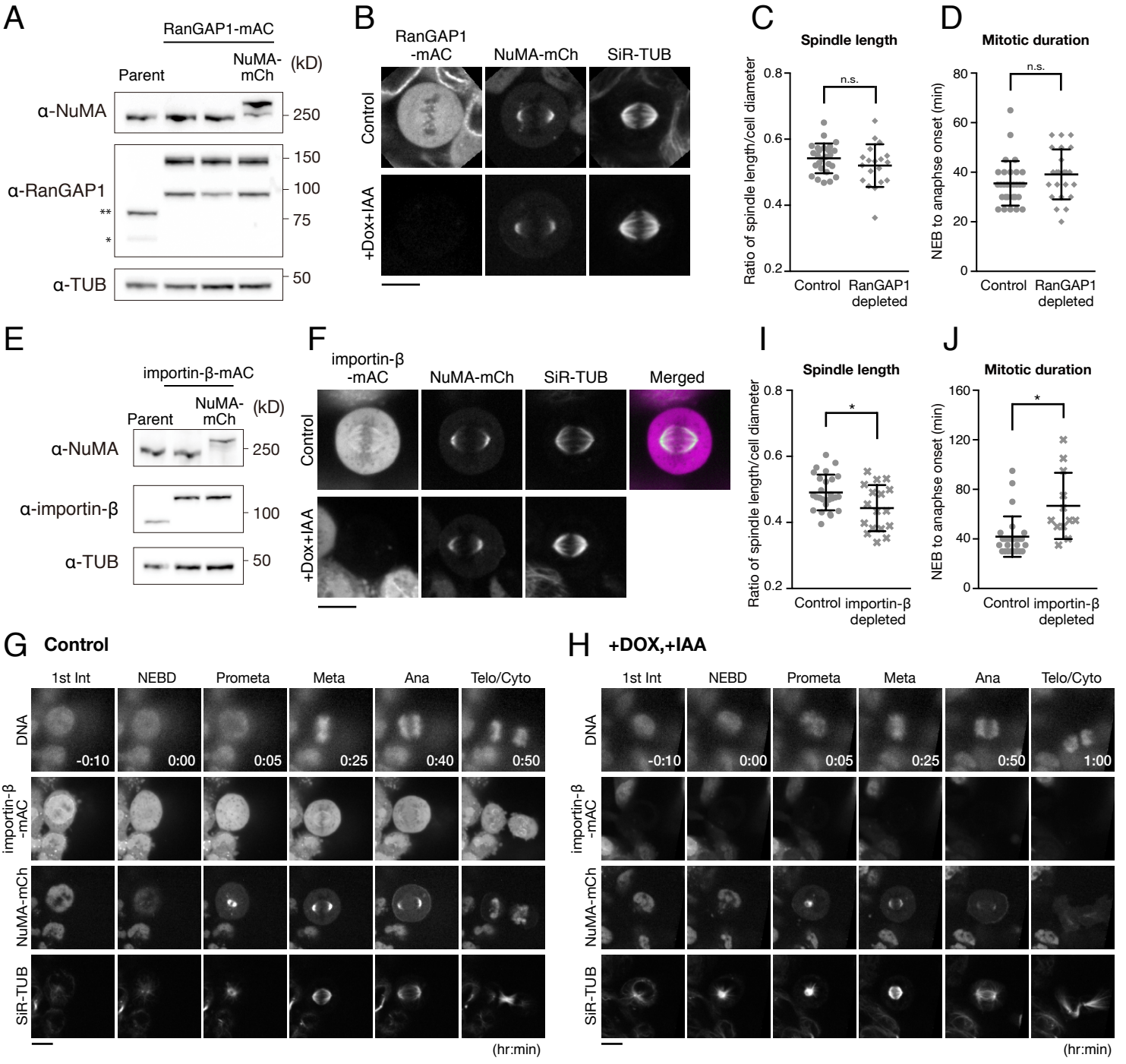

Figure 2. Depletion phenotypes of importin-β are similar to those of RCC1 but not RanGAP1.

(A) Immunoblotting for anti-NuMA, anti-RanGAP1 and anti-α-tubulin (TUB, loading control) showing bi-allelic insertion of the indicated tags. * and ** indicate RanGAP1 and SUMO-1 conjugated RanGAP1, respectively. (B) Metaphase RanGAP1-mAC cells showing live fluorescent images of RanGAP1-mAC, NuMA-mCherry (mCh), and SiR-tubulin (SiR-TUB) after 24 hrs following treatment with Dox and IAA. (C) Scatterplots of the ratio of spindle length and cell diameter in control (0.54 ± 0.04, n=26) and RanGAP1-depleted (0.52 ± 0.07, n=19) cells. (D) Scatterplots of mitotic duration (NEBD to anaphase onset) in control (35.5 ± 9.0, n=29) and RanGAP1-depleted (39.1 ± 10.1, n=23) cells. Bars in (C) and (D) indicate mean ± SD from >3 independent experiments. The differences were not statistically significant based on Welch's t-test in C (p=0.2108) and D (p=0.1851). (E) Western blot detection using anti-NuMA, anti-importin-β and anti-α-tubulin antibodies (TUB, loading control) showing bi-allelic insertion of the indicated tags. (F) Metaphase importin-β-mAC cells showing live fluorescent images of importin-β-mAC, NuMA-mCherry (mCh), and SiR-tubulin (SiR-TUB) following 24 hrs of Dox and IAA treatment. (G, H) Live fluorescent images of DNA (Hoechst 33342 staining), importin-β-mAC, NuMA-mCh, and SiR-TUB in control (G) and importin-β-depleted (H) cells. (I) Scatterplots of the ratio of spindle length and cell diameter in control (0.49 ± 0,05, n=26) and importin-β-depleted (0.44 ± 0.07, n=17) cells. (J) Scatterplots of mitotic duration (NEBD to anaphase onset) in control (41.9 ± 16.3, n=27) and importin-β-depleted (66.7 ± 26.7, n=12) cells. Bars in (G) and (H) indicate mean ± SD from >3 independent experiments. * indicates statistical significance according to Welch's t-test ($p<0.05$) in (I) and (J). Scale bars = 10 μm.

Figure 3

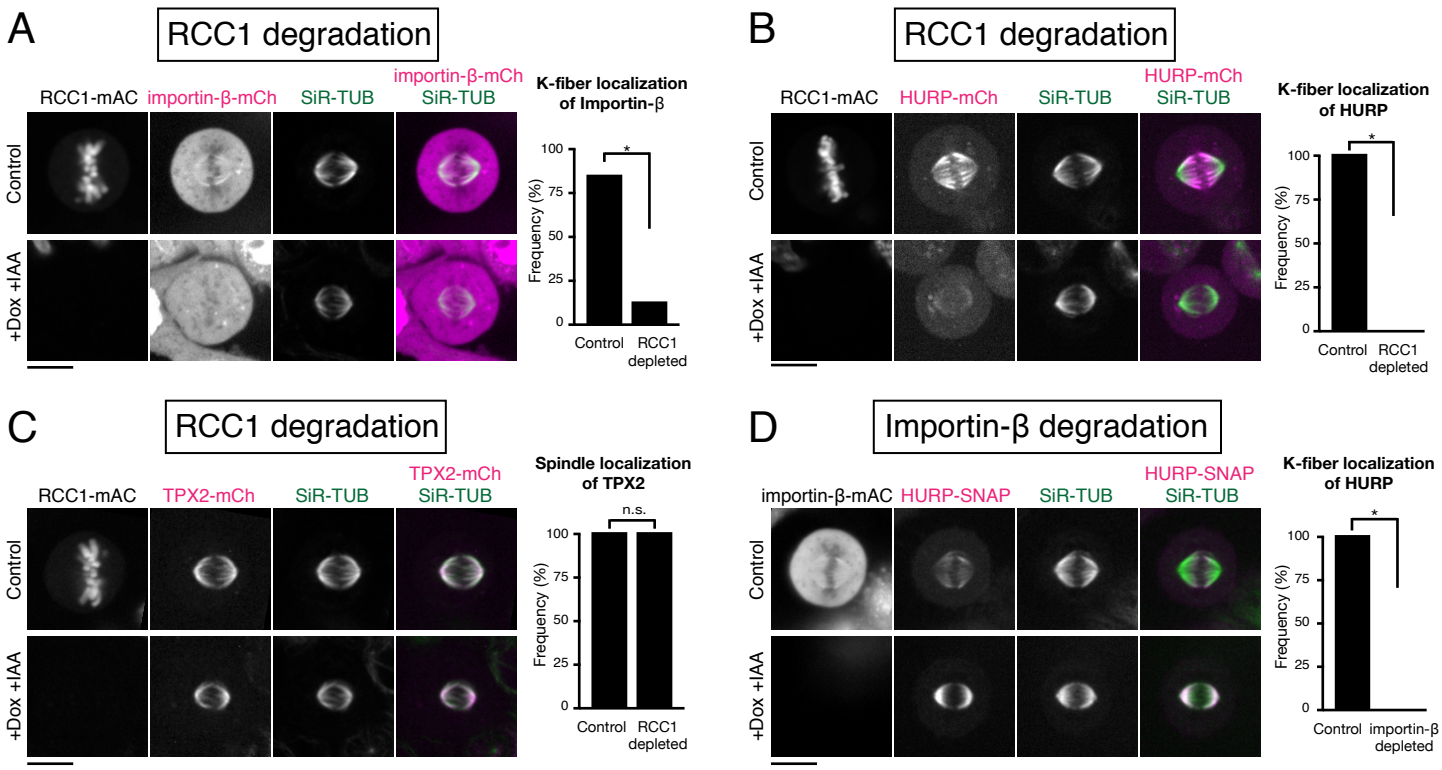

Figure 3. RCC1 and importin-β are required for HURP localization to k-fibers.

(A-C) Left: Metaphase RCC1-mAC cells showing live fluorescent images of RCC1-mAC, SiR-TUB and importin-β-mCherry (mCh) (A), HURP-mCh (B) and TPX2-mCh (C) after 24 hrs following treatment with Dox and IAA. Right: Quantification of k-fiber or spindle localization of importin-β, HURP, or TPX2 in control (n>40) and RCC1-depleted (n>40) cells from 3 independent experiments. (D) Left: metaphase importin-β-mAC cells showing live fluorescent images of importin-β-mAC, HURP-SNAP and SiR-TUB after 24 hrs following treatment with Dox and IAA. Right: quantification of k-fiber localization of HURP in control (n=49) and importin-β-depleted (n=43) cells from 3 independent experiments. * indicates statistical significance according to Z-test (99.9% confidence interval) in (A), (B) and (D). Scale bars = 10 μm.

Figure 4

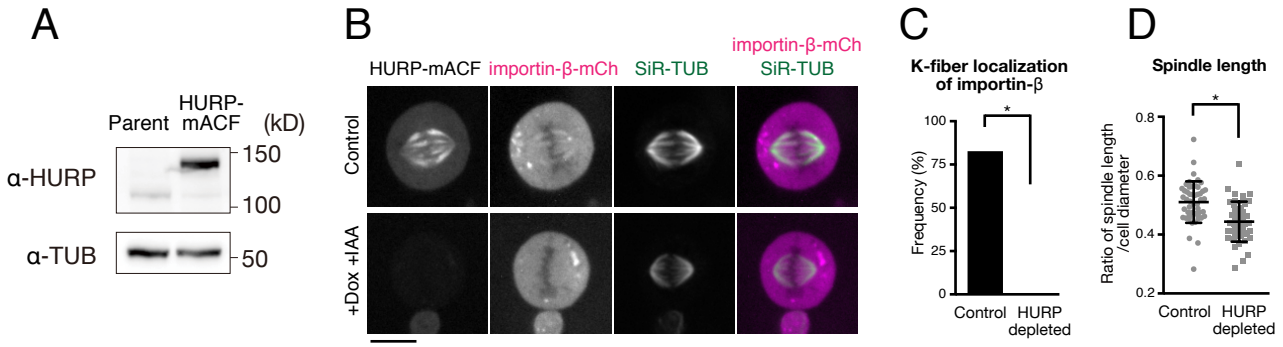

Figure 4. HURP is required to target importin-β to k-fibers and control proper metaphase spindle length.

(A) Immunoblotting for anti-HURP and anti-α-tubulin (TUB, loading control) showing bi-allelic insertion of the indicated tags. (B) Metaphase HURP-mACF cell lines showing live fluorescent images of HURP-mACF, importin-β-mCh and SiR-TUB after 24 hrs following Dox and IAA treatment. (C) Quantification of k-fiber localization of importin-β in control (n=49) and HURP-depleted (n=46) cells from 3 independent experiments. * indicates statistical significance according to Z-test (99.9% confidence interval). (D) Scatterplots of the ratio of spindle length and cell diameter in control (0.64 ± 0.05, n=49) and HURP-depleted (0.52 ± 0.06, n=43) cells. * indicates statistical significance according to Welch's t-test ($p<0.0001$). Scale bars = 10 μm.

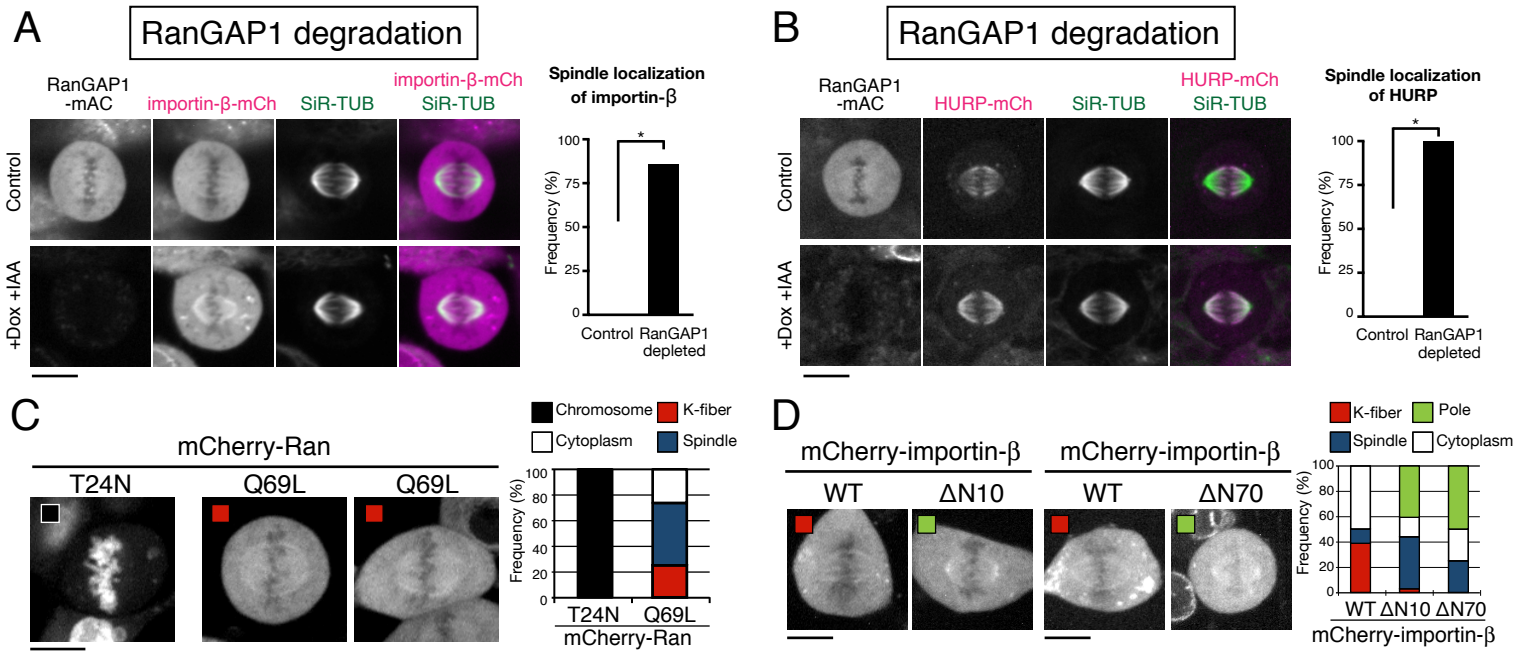

Figure 5. Ran-GTP binding to importin-β is required for k-fiber localization of importin-β

(A, B) Left: metaphase RanGAP1-mAC cells showing live fluorescent images of RanGAP1-mAC, SiR-TUB and importin-β-mCh (A) or HURP-mCh (B) after 24 hrs following Dox and IAA treatment. Right: quantification of k-fiber localization of importin-β or HURP in control (n=45) and RanGAP1-depleted (n>45) cells from 3 independent experiments. * indicates statistical significance according to Z-test (99.9% confidence interval). (C) Left: metaphase HEK293 cells expressing the mCherry-Ran mutants, T24N or Q69L. Right: quantification of mitotic localization of RanT24N (n=30) and RanQ69L (n=45). Maximally projected images from 5 z-sections are shown. (D) Left: metaphase HEK293 cells expressing mCherry-importin-β WT or the mutants, ΔN10 and ΔN70. Right: quantification of mitotic localization of importin-β WT (n=62), ΔN10 (n=32) and ΔN70 (n=16). Maximally projected images from five or three z-sections are shown in the 1st and 2nd panels or in the 3rd and 4th panels, respectively. Scale bars = 10 μm.

Figure 6

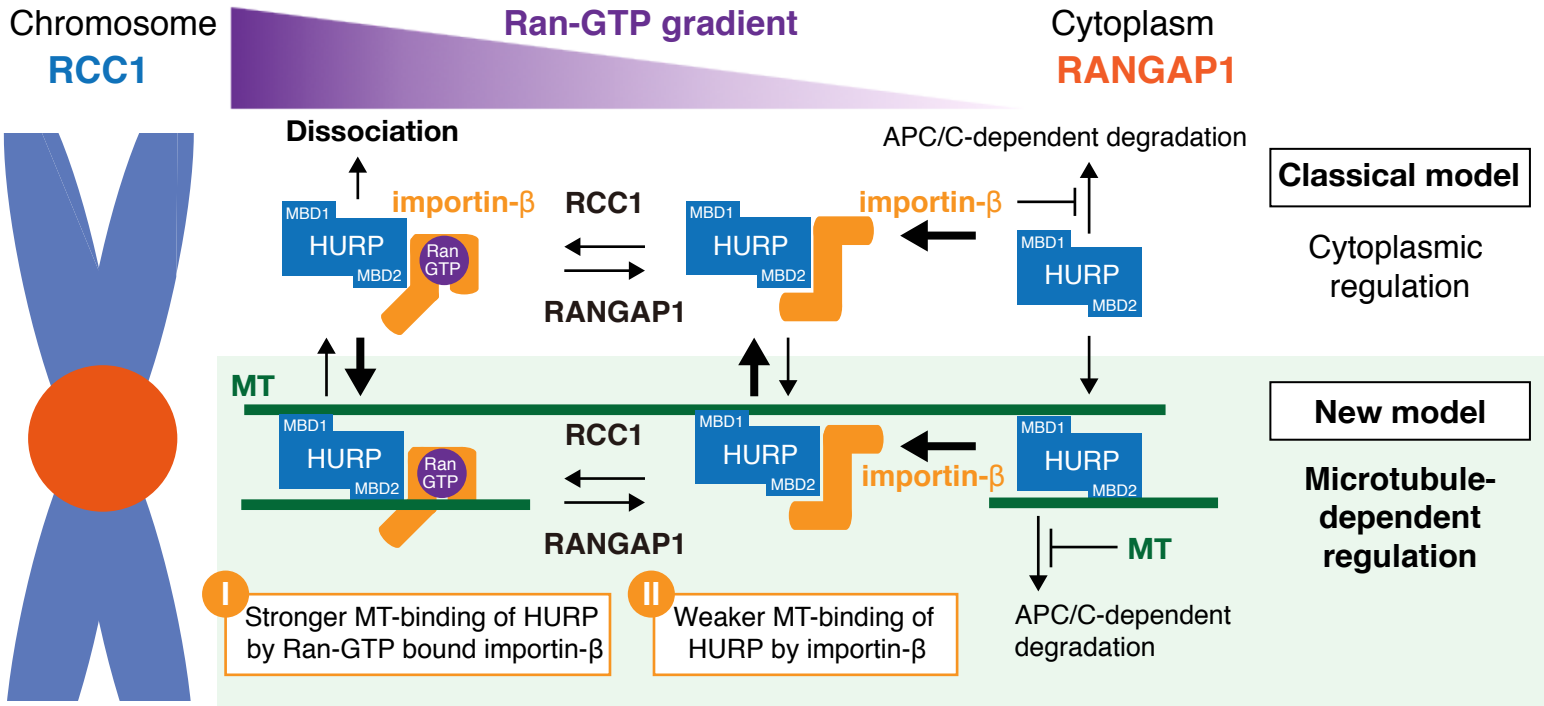

Figure 6. Proposed models of Ran-GTP based regulation of HURP-importin-β complexes

According to the classical model, in the cytoplasm, Ran-GTP binding to importin-β dissociates HURP from importin-β, as described previously (Sillje et al., 2006). In the proposed New Model, in the presence of microtubules, Ran-GTP binding to HURP-importin-β complexes induces a conformational change in importin-β and the ternary complexes would interact more strongly with the microtubules via both MBD1 and MBD2 domains of HURP (New model-I). On spindle microtubules around the spindle pole, Ran-GTP is hydrolyzed by cytoplasmic RanGAP1, and importin-β binding to HURP masks the MBD2 domain, resulting in reduced microtubule affinity of HURP (New model-II). Thus, the dual functions of importin-β in response to Ran-GTP gradient achieve k-fiber accumulation of HURP near the chromosomes. Both importin-β and microtubule act as a protector of HURP from APC/C-dependent degradation by masking the APC/C recognition motif in the MBD2 of HURP (Song et al., 2014).

Supplemental Figure S1

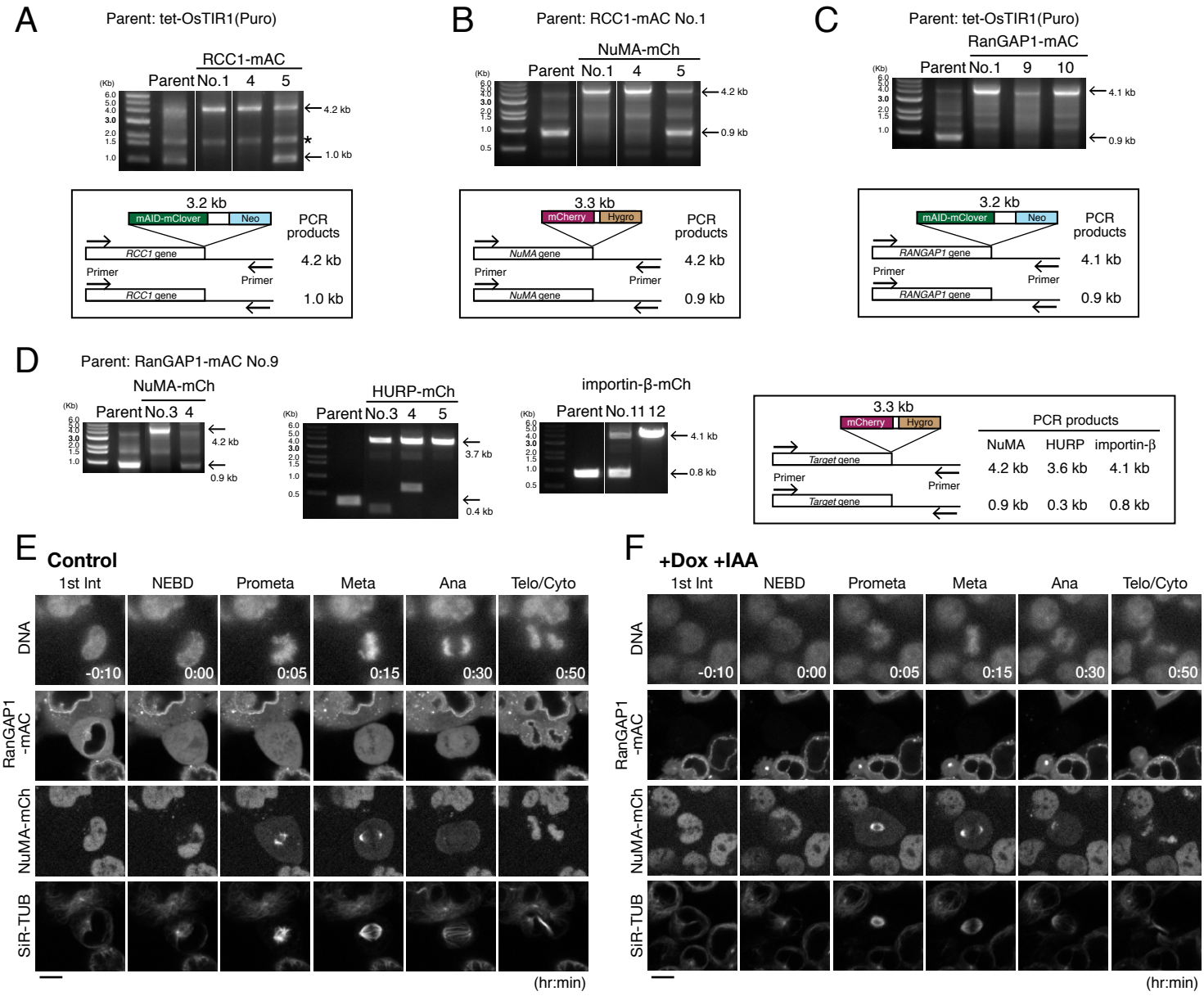

Figure S1. Generation of cell lines for auxin-inducible degaradation of endogenous RCC1 and RanGAP1

(A) Genomic PCR showing clone genotypes after neomycin (Neo) selection. Clone No.1 was used as a parental cell in the second selections. * indicates a non-specific band. (B) Genomic PCR showing clone genotypes after hygromycin (Hygro) selection. Clone No.1 was used in this study. (C) Genomic PCR showing clone genotypes after neomycin (Neo) selection. The clone No.9 was used as a parental cell in the second selections. (D) Genomic PCR showing clone genotypes after hygromycin (Hygro) selection. The clones No.3 (NuMA-mCh), No.5 (HURP-mCh), and No.12 (importin-β-mCh) were used, respectively. (E, F) Live fluorescent images of DNA (Hoechst 33342 staining), RanGAP1-mAC, NuMA-mCh, and SiR-TUB in control (E) and RanGAP1-depleted (F) cells. Scale bars = 10 μm.

Supplemental Figure S2

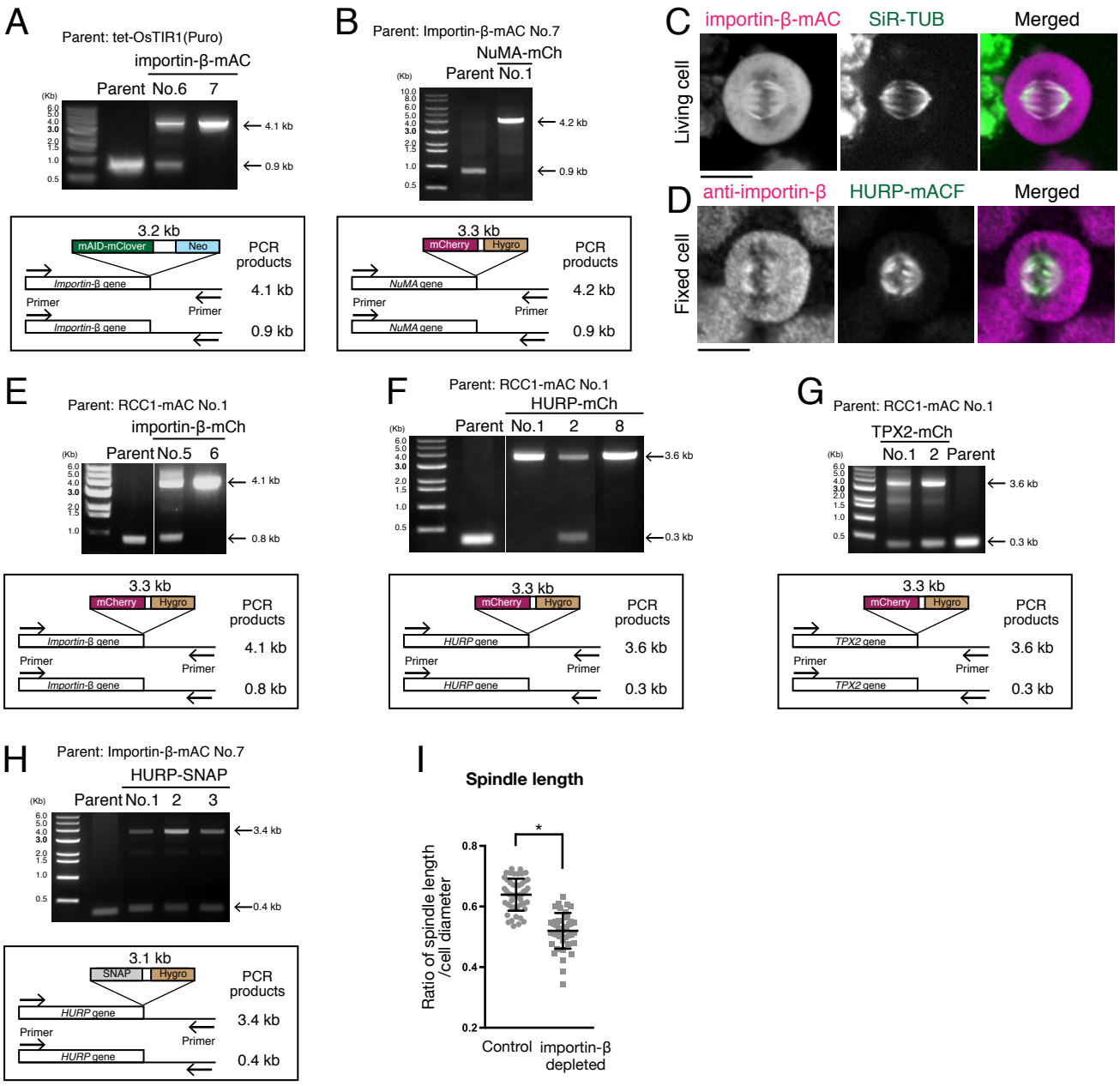

Figure S2. Generation of cell lines for auxin-inducible degaradation of endogenous importin-β

(A) Genomic PCR showing clone genotypes after neomycin (Neo) selection. The clone No.7 was used as a parental cell in the second selections. (B) Genomic PCR showing clone genotype after hygromycin (Hygro) selection. Clone No.1 was selected for further use. (C) Metaphase importin-β-mAC cells showing live fluorescent images of importin-β-mAC, and SiR-TUB. Single z-section images are shown. (D) Immunofluorescence images of fixed metaphase cells showing k-fiber localization endogenous importin-β and mAID-tagged HURP (HURP-mACF). The maximally projected images from 3 z-sections are shown. (E-H) Genomic PCRs showing clone genotypes after hygromycin (Hygro) selections. Clones No.6 (E), No. 8 (F), No.1 (G), and No.3 (H) were used. The mCherry or SNAP cassette was inserted into only one copy of TPX2 (G), or HURP (H) gene loci, respectively. (I) Scatterplots of the ratio of spindle length and cell diameter in the cell line expressing importin-β-mAC and HURP-SNAP: control (0.52 ± 0.07, n=49) and importin-β-depleted (0.44 ± 0.07, n=46) cells. * indicates statistical significance according to Welch's t-test ($p<0.0001$).

Supplemental Figure S3

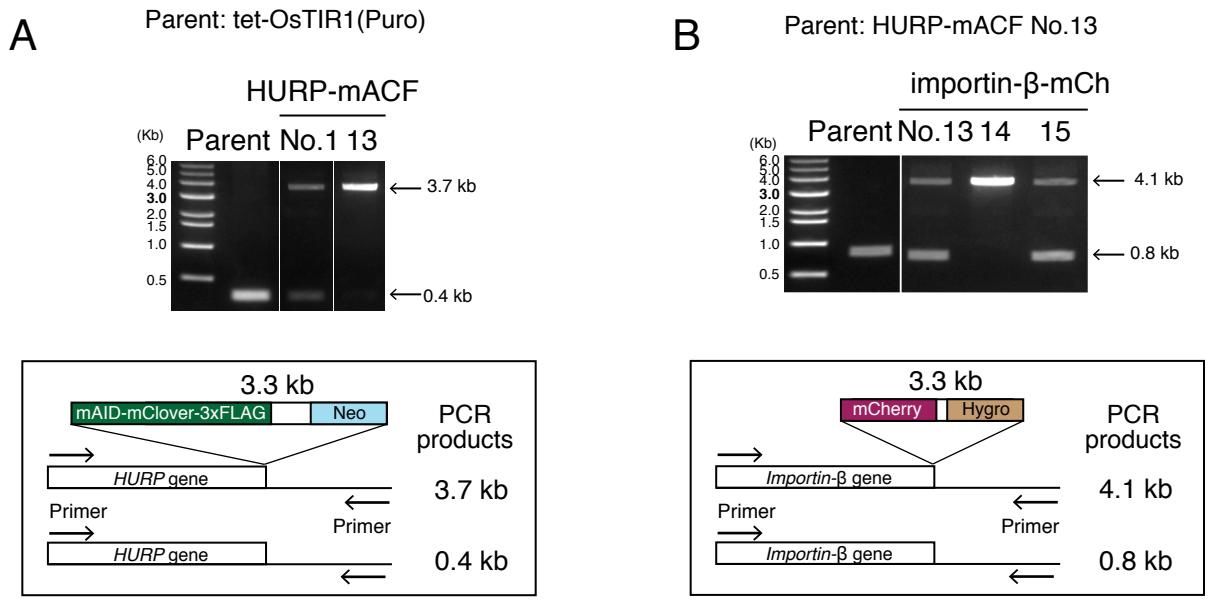

Figure S3. Generation of cell lines for auxin-induced degradation of endogenous HURP

(A) Genomic PCR showing clone genotype after neomycin (Neo) selection. Clone No.13 was used as a parental cell in the second selections. (B) Genomic PCR showing clone genotypes after hygromycin (Hygro) selection. Clone No.14 was used.

Supplemental Figure S4

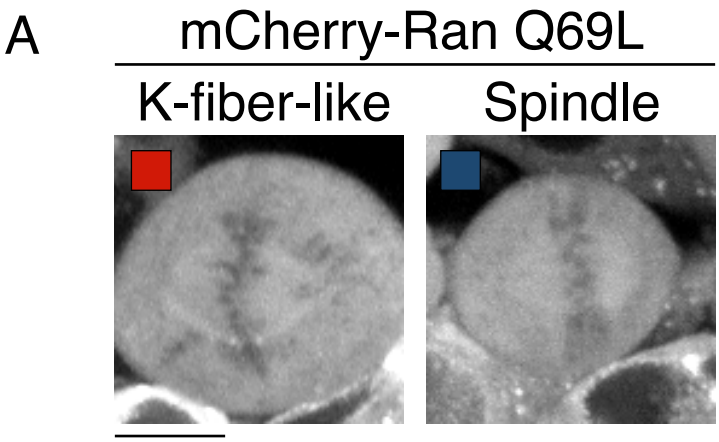

Figure S4. Mitotic localization of RanQ69L mutant

(A) Live fluorescent images of metaphase HEK293 cells transiently expressing the mCherry-RanQ69L mutant. About 25% of cells display k-fiber-like localization. In a few cases, kinetochore-like punctate signals were seen (left). About 50% of cells show spindle-like fuzzy localization (right).